



Contents lists available at ScienceDirect

Spectrochimica Acta Part A: Molecular and Biomolecular Spectroscopy

journal homepage: www.journals.elsevier.com/spectrochimica-acta-part-a-molecular-and-biomolecular-spectroscopy

Mueller matrix polarimetry reveals chiroptical properties of metal chelates in solutions

Daniel Vala^{a,b,*}, Jiří Zdráhala^{c,d}, Jana Hudecová^b, Hana Šestáková^{d,e}, Jaroslav Šebestík^d, David Kopečný^f, Josef Kapitán^b, Petr Bouř^{c,d,**}, Kamil Postava^{a,***}

^a Department of Materials Engineering and Recycling, Faculty of Materials Science and Technology, VSB – Technical University of Ostrava, 17. listopadu 2172/15, 708 00 Ostrava-Poruba, Czech Republic

^b Department of Optics, Palacký University Olomouc, 17. listopadu 1192/12, 779 00 Olomouc, Czech Republic

^c Department of Analytical Chemistry, University of Chemistry and Technology, Technická 5, 166 28 Prague, Czech Republic

^d Institute of Organic Chemistry and Biochemistry, Academy of Sciences, Flemingovo náměstí 542/2, 160 00 Prague, Czech Republic

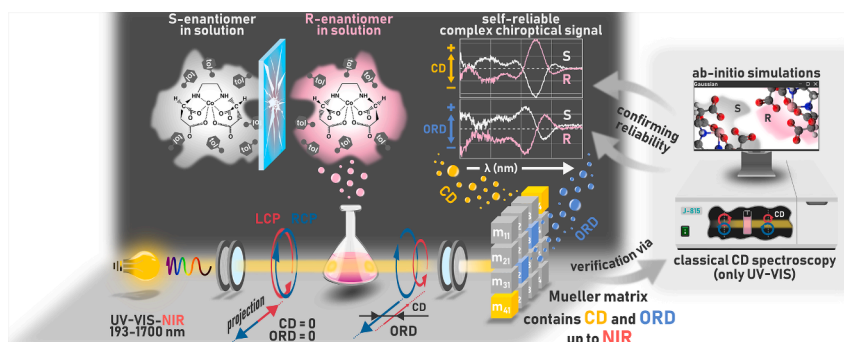
^e Department of Biochemistry and Microbiology, University of Chemistry and Technology, Technická 5, 166 28 Prague, Czech Republic

^f Department of Experimental Biology, Palacký University Olomouc, 17. listopadu 1192/12, 779 00 Olomouc, Czech Republic

HIGHLIGHTS

- Mueller polarimetry captures the complex chiroptical response of metal complexes.
- A strong chiral signal in the near infrared region was observed for a cobalt complex.
- Density functional theory enables to verify and interpret the observations.
- We develop optimal experimental protocols and discuss the limits of the technique.
- Kramers-Kronig self-consistency confirms the experimental datasets.

GRAPHICAL ABSTRACT



ARTICLE INFO

Keywords:

Mueller matrix polarimetry
Density functional theory
Circular dichroism
Transition metal complexes
Near-infrared spectroscopy
Kramers-Kronig transformation

ABSTRACT

Proper characterization of molecular chiroptical properties is vital for organic chemistry and drug development. Nonetheless, narrow spectral ranges and the necessity for specialized equipment often limit traditional methods such as optical rotatory dispersion and electronic circular dichroism. Here, we introduce Mueller matrix polarimetry (MMP) as a more versatile tool for chiroptical analysis, capable of simultaneously capturing circular dichroism and optical rotatory dispersion spectra across ultraviolet to near-infrared wavelengths in a single measurement. We applied MMP to chiral metal complexes of Al, Mn, and Co, commonly used as catalysts in asymmetric syntheses. Using a robust experimental methodology, MMP distinguished enantiomeric forms and provided reliable chiroptical information by leveraging the inherent relationship between circular dichroism and optical rotatory dispersion. We interpreted our findings on the basis of density functional theory simulations,

* Corresponding author at: Department of Materials Engineering and Recycling, Faculty of Materials Science and Technology, VSB – Technical University of Ostrava, 17. listopadu 2172/15, 708 00 Ostrava-Poruba, Czech Republic.

** Corresponding author at: Institute of Organic Chemistry and Biochemistry, Academy of Sciences, Flemingovo náměstí 542/2, 160 00 Prague, Czech Republic.

*** Corresponding author.

E-mail addresses: daniel.vala@upol.cz (D. Vala), bour@uochb.cas.cz (P. Bouř), kamil.postava@vsb.cz (K. Postava).

<https://doi.org/10.1016/j.saa.2025.126279>

Received 7 January 2025; Received in revised form 1 April 2025; Accepted 20 April 2025

Available online 21 April 2025

1386-1425/© 2025 The Authors. Published by Elsevier B.V. This is an open access article under the CC BY license (<http://creativecommons.org/licenses/by/4.0/>).

compared them to traditional electronic circular dichroism and absorption spectroscopies, and performed the Kramers-Kronig analysis. The combined approach of chiroptical MMP and ab-initio, for example, reveals delicate near-infrared chiroptical spectra of a neutral cobalt metal complex. Although MMP is more commonly used for solid state, the developed experimental protocol significantly expands its capabilities to solutions. It allows measurements without the need for both enantiomers and offers new insights into molecular chirality with potential applications across traditional and interdisciplinary branches of science and industry.

1. Introduction

Chirality, where objects exist in two mirror-reversed forms known as enantiomers, is exhibited by many life-forming molecules, affecting their shape, reactivity, and biocompatibility. Approximately 56 % of drugs marketed globally, including over-the-counter items like ibuprofen, are chiral [1,2]. Consequently, the pharmaceutical industry depends on robust and reliable methods for controlling the absolute configuration and enantiomeric purity of molecules, in extreme cases, to prevent incidents like the thalidomide tragedy [3,4]. Techniques such as X-ray crystallography [5,6], chiral chromatography [7–10], and advanced nuclear magnetic resonance [11,12] can determine the absolute configuration of a molecule. In specific cases, a faster, more straightforward, and more cost-effective approach to assess molecular chirality is to view it through its optical activity, such as electronic circular dichroism (ECD) and optical rotatory dispersion (ORD, also known as circular birefringence) spectroscopy. The signs and magnitudes of circular dichroism (CD) and ORD reflect the molecules' handedness and can be used to determine the enantiomeric excess in the studied sample. In addition to these electronic methods [13], chiroptical spectroscopies further include vibrational circular dichroism (VCD) [14] and Raman optical activity (ROA) [15,16]. These are easier to model computationally but suffer from limited sensitivity.

Despite the successful demonstration of ORD-enhanced VCD spectroscopy [17], none of these methods are nowadays practical for simultaneous measurement of ORD and CD. The weakness of the chiroptical signal often necessitates the measurement of both enantiomers of a chiral molecule to confirm the data through “mirror symmetry” in the spectra or verify the findings for one enantiomer via theoretical simulations. However, extended molecular size or complexity of the sample can make the ab-initio modelling challenging and resource-intensive. Obtaining both enantiomers for analysis can be technically and financially demanding.

Another possibility for verifying experimental data is to measure CD and optical rotatory dispersion ORD simultaneously, treating them as the imaginary and real parts of a single complex chiroptical signal. According to the Kramers–Kronig (KK) relations [18–21], these two components are mutually consistent for any causal linear dielectric response [22]. The KK relations can thus be used to check reliability of the chiroptical signal, similarly as measurements with both enantiomers.

Several specialized chiroptical techniques have been developed to acquire CD and ORD spectra simultaneously. However, time-resolved CD [23,24] and interferometric methods [25], for example, are usually limited to the ultraviolet–visible (UV–VIS) region [24,26], and may overlook key chiroptical features outside the strongest absorption bands [27,28]. Second, these methods often require tedious calculations and intensive data post-processing, partly because parasitic linear birefringence from the sample or setup can overshadow the inherent chiroptical signal [29].

High-accuracy universal polarimetry (HAUP) offers another solution for measuring the complex chiroptical response, as it can separate fundamental polarimetric effects – linear dichroism, linear birefringence, CD, and ORD – with exceptional precision [30,31]. Those systems are successfully employed for analysis of (bio)organic anisotropic crystals [32], accurately resolving their fundamental polarimetric properties including optical activity [33], gyration tensor components [34], and magneto-optics effects [35]. However, HAUP systems require numerical

fitting of intensity data to Jones-matrix-based coherent models. Therefore, they inherently cannot measure depolarization, necessitating thus samples that are thin, smooth, and non-scattering. Modern generalized-HAUP instruments [36] may incorporate CCD detection over limited UV–VIS ranges, reducing measurement times from 24 h to approximately 90 min [37]. Nonetheless, this is still a lengthy process because HAUP requires measuring several polarizer-analyzer configurations, further limiting the samples to those exhibiting only slowly varying optical properties. This further limits HAUP's suitability for time-dependent phenomena or routine high-throughput measurements.

Furthermore, all the setups discussed are custom-built with custom-developed software, which makes those techniques less available to the broader user community.

Mueller matrix polarimetry (MMP) overcomes many of the discussed limitations. Regardless of the instrumentation, its core concept is straightforward: continuously modulate the polarization state of the incident light, let it interact with the sample, and measure the resulting change in the polarization at the output. In other words, the MMP captures the complete polarization response of a sample, which encodes its full optical characteristics. MMP is particularly sensitive to the phase differences between left and right circular polarizations and changes in their ellipticity. The information gathered can be directly converted into ORD and CD. The complex chiroptical response is extracted from the 4×4 Mueller matrix \mathbb{M} (MM), which is a real-valued experimental observable connecting 4-component input and output Stokes vectors,

$$\mathbf{S}_{\text{out}} = \mathbb{M}\mathbf{S}_{\text{in}}. \quad (1)$$

Although the MM complexity increases with the complexity of a sample, it remains manageable for typical matter investigated in “classical” chiroptical spectroscopy, e.g., a solutions of chiral molecules. Such samples do not significantly depolarize or scatter light and MM simplifies to a matrix with distinct CD, ORD, linear dichroism, and linear birefringence elements. Unlike for HAUP, there is no need for numerical fitting as the polarimetric effects emerge directly from the measured matrix.

Modern MMP or ellipsometric instruments – commonly based on pairs of rotating compensators (RC2) or photoelastic modulators (PEM) – can, in principle, detect all these effects and depolarization. They proved useful in traditional thin-film metrology [38–40], probing layers down to a few nanometers [41–43]. They are also applied in less conventional contexts, ranging from cancer diagnostics [44–46] and ultrafast electronic phenomena [47,48] to in vivo imaging [49,50], solar and hydrogen energy harvesting [51–53], and metasurface-based optics control [54]. In many of these applications, the signals are weak and complicated by depolarization or scattering; however, modern instruments are increasingly adept at disentangling these challenges. Such systems are typically versatile in terms of the samples (capable of measuring gases, liquids, powders, and solids), modular (allowing for customized setups), fast (complete polarization analysis in fractions of a second), and broadband (covering UV to near-IR or even mid-IR). User-friendly commercial software makes them attractive both to experts and casual users.

While MMP is well established in the analysis of chiral anisotropic systems such as crystals [55], thin films [56,57], nanowire assemblies [58], and specific biological samples [59,60], solutions are less explored. In them, the chiroptical signals are typically weaker and more challenging to detect, especially near strong absorption bands.

PEM-based Mueller matrix polarimeters typically offer higher sensitivity than RC2 setups. For example, PEM-based analyses of molecular solutions have been successfully used for time-dependent optical rotatory dispersion (ORD) measurements during crystallization [61], as well as for comprehensive polarimetric studies of porphyrin aggregates [62] that undergo chirality switching [63]. Nonetheless, the applications are still relatively limited, often restrained to specific systems, and primarily confined to monochromatic or UV–VIS ranges. For RC2, systematic methodological studies of CD and ORD of chiral molecular solutions over a wide spectral range are now known to us.

We applied RC2-based MMP to chiral salen-metal and salen-chelate complexes to explore their complex chiroptical signal. The studied compounds are commonly used as chiral catalysts in asymmetric syntheses such as Jacobsen epoxidation [64], agents for electrochemical reductions [65], or are recommended standards for chiroptical spectroscopy [66]. The molecules are relatively rigid and small, allowing for reasonably precise density functional theory (DFT) simulations of their spectra, providing signals across a wide range of wavelengths. Moreover, both enantiomers are available. It turned out that, when accessible ranges overlap, the results from a commercial Woollam RC2-DI system compare well to spectra from dedicated ECD instruments, proving the viability of the MMP approach and bringing more information about ORD. Notably, the near infrared (NIR) chiroptical signal is measured and calculated for the first time for neutral Co-salen; previously, such spectra have only been reported for oxidized Co-salen or Co-salen with substituents other than *tert*-butyl at the salicylidene group or modifications to the central cobalt [67–69]. To rule out any ambiguity or potential instabilities of the investigated system caused by the choice of the solvent, we present a comparison of spectra for cobalt salen complex enantiomers measured in toluene and dichloromethane. Indeed, the NIR signal lies outside the traditional ECD range but can be assigned using DFT calculations. MMP thus can also be considered complementary to ECD, unveiling additional chiroptical response and information about a sample.

The outline of the present article is as follows: Section 2 details the experimental procedures, sample preparations, and theoretical simulations, comparing the concept of the Mueller matrix with classical chiroptical spectroscopy. Section 3.1 introduces the experimental methodology of chiral MMP measurements, noting some aspects that are critical but rather unconventional for non-chiral polarimetry or ellipsometry. It addresses typical experimental characteristics emerging in typical experimental MMs, various types of systematic errors, and strategies for their mitigation and elimination. For this, we illustrate our approach to the cobalt-salen salt. Section 3.2 reveals its NIR chiroptical signal measured and ab-initio simulated in different solvents, uncovering its solvatochromic properties. The aim of Section 3.3 is to validate the proposed MMP approach against more established ECD measurements and DFT simulations using a sample with a strong chiroptical signal over ultraviolet and visible wavelengths. We explain the benefits of MMP's accessibility to the complex chiroptical signal by providing the Kramers-Kronig analysis of different MMP and ECD datasets. Section 3.4 further explores the chiroptical analysis of other salen complexes while investigating MMP's sensitivity limitations. A more detailed analysis of the sensitivity and reliability is in Section 4, which also explains how the ellipsometer instrumentation impacts the accuracy in the data acquisition.

2. Samples and experimental methods

2.1. Materials

(*S,S*) and (*R,R*) enantiomers of the following compounds were purchased from Sigma-Aldrich; their molecular structures are shown in Fig. 1: *N,N'*-Bis(3,5-di-*tert*-butylsalicylidene)-1,2-cyclohexanediaminoaluminium(III) chloride (hereafter abbreviated as *S/R*-AlCl-salen, $M_{\text{AlCl-salen}} = 607.26$ g/mol, a yellow powder, Fig. 1a); *N,N'*-Bis(3,5-di-

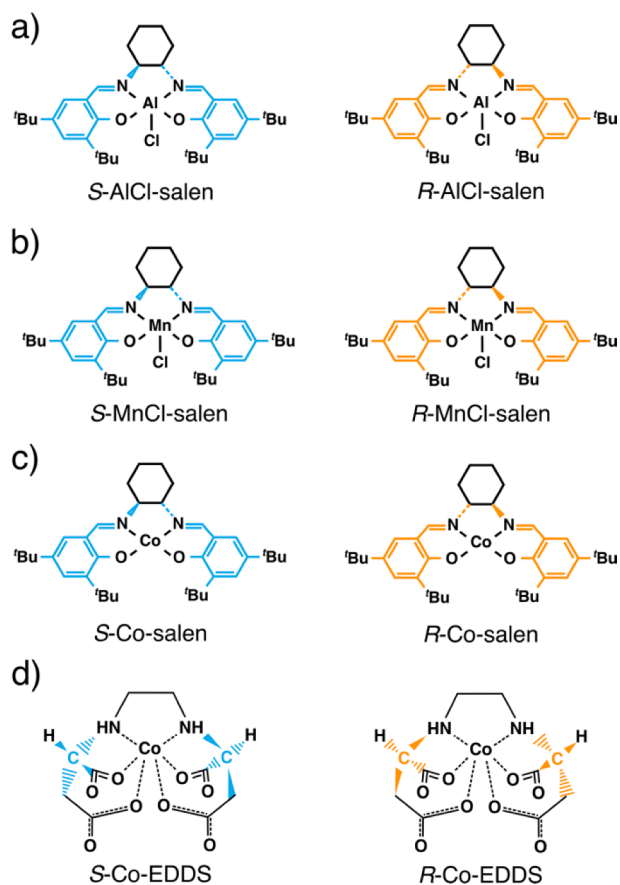


Fig. 1. Investigated systems: a) (*S,S*)- and (*R,R*)-*N,N'*-Bis(3,5-di-*tert*-butylsalicylidene)-1,2-cyclohexanediaminoaluminium(III) chlorides. b) (*S,S*)- and (*R,R*)-*N,N'*-Bis(3,5-di-*tert*-butylsalicylidene)-1,2-cyclohexanediaminomanganese(III) chlorides. c) (*S,S*)- and (*R,R*)-*N,N'*-Bis(3,5-di-*tert*-butylsalicylidene)-1,2-cyclohexanediaminocobalt(II), and d) (*S,S*)- and (*R,R*)-*N,N'*-ethylenediaminedisuccinic cobalt(III) complexes.

tert-butylsalicylidene)-1,2-cyclohexanediaminomanganese(III) chloride (Jacobsen catalyst or *S/R*-MnCl-salen, $M_{\text{MnCl-salen}} = 635.20$ g/mol, brownish powder, Fig. 1b); *N,N'*-Bis(3,5-di-*tert*-butylsalicylidene)-1,2-cyclohexanediaminocobalt(II) (*S/R*-Co-salen, $M_{\text{Co-salen}} = 603.74$ g/mol, red powder, Fig. 1c). The complexes were used without further purification.

The AlCl and MnCl-salen complexes were dissolved in toluene (>99 %, Penta) to prepare stock solutions of 10 mg/ml (16.47, 15.74 μM , respectively). Solutions at concentrations of $c = 5, 2.5, 1.25, 0.625$, and 0.3125 mg/ml (concentrations in μM scales by a factor 0.5 as well) were prepared by direct dilution from stock solution using separate volumetric flasks for each concentration level. All concentrations were used for the ellipsometric measurements; used concentrations for ECD measurements are specified for each sample in the following text. The Co-salen complexes were dissolved in toluene (≥ 99.9 %, Sigma-Aldrich, product no. 650579) and dichloromethane (≥ 99.9 %, Supelco, product no. 106048). Solutions were prepared by direct dilution to concentrations $C = 5, 2.5, 1.25, 0.625$ mg/ml (8.28, 4.14, 2.07, 1.035 μM) for toluene and $c = 5, 1.25, 0.625$ mg/ml for dichloromethane solutions.

Co(III) complexes with (*S,S*)- and (*R,R*)-*N,N'*-ethylenediamine disuccinic anion (*R/S*-Co-EDDS, $M_{\text{Co-EDDS}} = 349.16$ g/mol Fig. 1d) were synthesized as described in Refs. [66,70] and investigated as aqueous solutions at concentrations of 5.242 mM and 5.008 mM, respectively.

2.2. Ab-initio modeling

Program Gaussian was used for all quantum chemical calculations, adopting density functional theory (DFT) [71]. Ground state geometries of the complexes were optimized by energy minimization; multiplicities found for the lowest energy structures were AlCl-salen: 1; MnCl-salen: 5; Co-salen: 2; Co-EDDS: 1. Absorption, ORD and CD spectra were obtained using time-dependent DFT (TD-DFT). Solvent effects were included with the polarizable continuum model (PCM) for toluene and dichloromethane and conductor-like solvent model (COSMO) for water. The B3LYP hybrid functional [72] with the 6-311++G** basis set [73,74] was applied by default. Several other levels of theory were tried: B3LYP/6-311+G*, B3LYP/def2-TZVP [75], CAM-B3LYP/6-311++G** [76], and B3PW91 [72]/6-311++G**. Similarity indices for the experimental and calculated spectra were calculated as listed in the Supplementary Information (SI), Table S1.

For all complexes, the electronic spectra were calculated without vibrational resolution, i.e., in the vertical approximation. The intensities were then convoluted with Gaussian line shapes with full width at half maximum (FWHM) $\Delta\omega = 3000 \text{ cm}^{-1}$ (constant in energy scale), except for Co-salen where 80 nm was used.

In addition, to explain the experimental bands around 1200 nm observed for Co-salen, vibrational splitting was simulated within the time-independent framework, using the vertical Hessian method [77], where the electronic excited state vibrational frequencies were calculated at the electronic ground state geometries. Temperature effects at 298.15 K and Herzberg-Teller terms were included.

2.3. UV-VIS and CD

UV/VIS absorption measurements were conducted on a Jasco V-760 double-beam spectrophotometer at room temperature, using CD-quality (stress-free) 1 mm quartz cuvettes STARNA. The spectrophotometer operates within the spectral range of 178–800 nm, and the samples were measured with pure solvent reference. UV/VIS/NIR absorption spectra of Co-salen were conducted using an Agilent Cary7000 double-beam spectrophotometer using 1 mm CD-quartz cuvettes STARNA measured with pure solvent as a reference.

CD spectra were measured at Jasco J-815 in a spectral range of 300–800 nm using 1 mm CD-quartz cuvettes STARNA against pure solvent. Each spectrum was obtained as an average of three scans taken with a resolution of 1 nm and scanning speed of 100–200 nm/min.

There were measured different concentrations for each sample to access CD in the whole spectral range: 5 mg/ml and 0.625 mg/ml for MnCl-salen; 0.625 mg/ml for AlCl-salen; 5, 2.5, 1.25, and 0.625 mg/ml for Co-salen. All measurements were performed at room temperature.

2.4. Chiroptical response in the Mueller matrix

The polarimetric measurements were performed on a commercial system Woollam RC2-DI Mueller matrix spectroscopic ellipsometer (cf. the simplified scheme in Fig. 2a) with a spectral range of 193–1700 nm using a 10 mm STARNA cuvette for salens and 2, 5 and 10 mm STARNA cuvettes for Co-EDDS. Note that Mueller matrix spectroscopic ellipsometry in transmission geometry is typically called Mueller matrix polarimetry, whereas “ellipsometry” is generally reserved for specular reflection measurements. The chiroptical spectra were extracted from the experimental Mueller matrices measured in the transmission configuration at normal angle of incidence. The non-normalized Mueller matrix \mathbb{M} in Eq. (1) is an experimental quantity that fully characterizes how the arbitrary elliptical polarization state of the light is transformed upon interaction (reflection or transmission) with a material. Each element of the MM provides information about different aspects of the light-matter interaction, including depolarization (loss of coherence), diattenuation (differential absorption between orthogonal polarization states), and retardation (phase shifts between those states). Diluted molecular solutions are non-depolarizing, non-scattering and without effects of linear dichroism and linear birefringence. The Mueller matrix \mathbb{M} in Eq. (1) is then defined as [61,78–80]

$$\mathbb{M} = e^{-2\kappa'} \begin{bmatrix} \cosh\Gamma' & 0 & 0 & \sinh\Gamma' \\ 0 & \cos\Gamma & \sin\Gamma & 0 \\ 0 & -\sin\Gamma & \cos\Gamma & 0 \\ \sinh\Gamma' & 0 & 0 & \cosh\Gamma' \end{bmatrix} \quad (2)$$

Detailed derivation of this matrix can be found in Supplementary Information. Parameter κ' is the isotropic absorption of the medium, quantities Γ and Γ' constitute the complex phase difference $\tilde{\Gamma} = \Gamma - i\Gamma'$ between left (L) and right (R) circular polarizations, and are respectively defined as

$$\Gamma = \frac{2\pi}{\lambda} (n_L - n_R) d, \quad (3a)$$

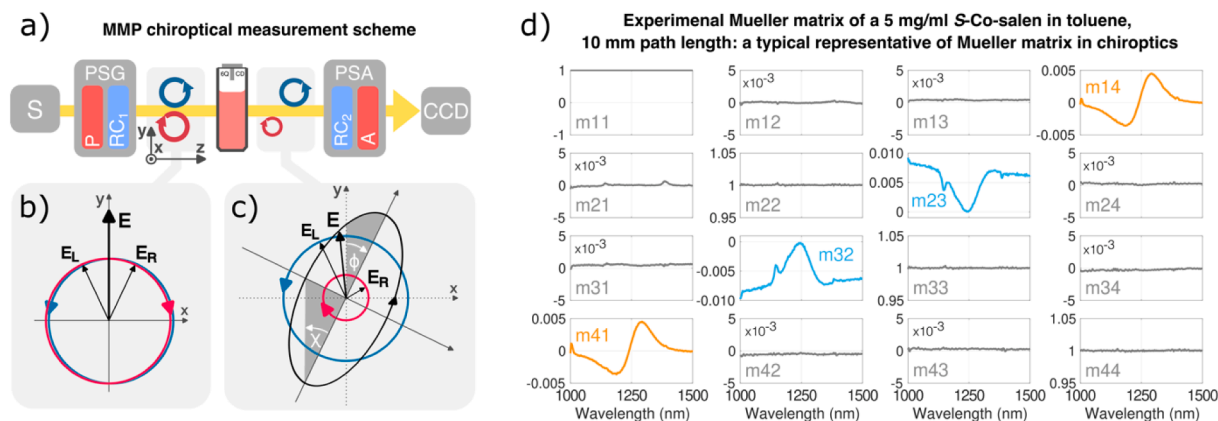


Fig. 2. a) The MMP transmission setup used for chiroptical analysis. Light from the source (S) is continuously polarized by a polarization state generator (PSG) consisting of a polarizer (P) and a rotating compensator (RC1) to many different polarization states. As the light interacts with a sample (cuvette containing a chiral solution), it undergoes changes in polarization, which are decoded by a polarization state analyzer (PSA) that includes an analyzer and a rotating compensator (RC2) and detected at the CCD camera. b) For the initial state, the electric field vectors E_L and E_R representing left- and right-circular polarizations combine to a linear polarization. c) Interaction with a chiral sample induces differential absorption and phase retardation between these components, resulting in the E_L and E_R vector projections summing into a polarization ellipse characterized by an ellipticity angle χ and a fast-axis orientation ϕ . d) Example of an experimental Mueller matrix. The symmetric elements m_{14} , m_{41} indicate CD, while the antisymmetric elements m_{23} , m_{32} represent ORD.

$$\Gamma' = \frac{2\pi}{\lambda} (n'_{\text{L}} - n'_{\text{R}})d. \quad (3b)$$

They depend on the wavelength λ , thickness of the medium d and refractive indices $n_{\text{L,R}}$ and absorption coefficients $n'_{\text{L,R}}$ for L and R circular eigen-polarizations, which form the complex propagation constant $\tilde{n}_{\text{L,R}}(\lambda) = n_{\text{L,R}}(\lambda) - in'_{\text{L,R}}(\lambda)$. In classical ellipsometric literature, Γ and Γ' are usually the direct definitions of circular birefringence and circular dichroism, respectively [63].

All following MMs throughout this Article are normalized to the element m_{11} , which only describes transmitted intensity for unpolarized light (average intensity of all polarizations) and are abbreviated with bold capital **M**. Consequently, all elements of the normalized Mueller matrix range between -1 and $+1$. Additionally, we do not include the element m_{11} , as it cannot be extracted from the commercial instrument employed in this study. Nevertheless, normalized MMs provide the most convenient representation of the full polarimetric response because they enable meaningful comparisons across different systems.

In typical chiroptical measurements of molecular solutions, Γ and Γ' are much less than 1, facilitating the separation of CD and ORD signals into distinct MM elements. This assumption leads to

$$\Gamma = 2\phi, \quad (4a)$$

$$\Gamma' = 2\chi, \quad (4b)$$

where ϕ is the azimuthal rotation, and χ is its ellipticity angle of a transmitted polarization ellipse when the incident polarization is linear, see Fig. 2b,c. The sign of ϕ and χ reflect the handedness of a sample. Note, that if there is no absorption (circular dichroism), the plane of the emerging linear polarization rotates about the angle ϕ . However, assuming small CD and ORD and with use of (4), the matrix (2) simplifies (after normalization) to Mueller matrix,

$$\mathbf{M}(\Gamma', \Gamma \ll 1) = \begin{bmatrix} 1 & 0 & 0 & 2\chi \\ 0 & 1 & 2\phi & 0 \\ 0 & -2\phi & 1 & 0 \\ 2\chi & 0 & 0 & 1 \end{bmatrix}. \quad (5)$$

Fig. 2d represents a typical experimental example of the Mueller matrix (5) for the chiral solution of *S*-Co-salen. The spectra suggest the consistency with the KK relations, which will be further corroborated in Sec. 3.

Note that the polarimetric response of the cuvette containing the analyte is disregarded, which is acceptable only if there is no residual stress in the cuvette facets and if the cuvette perfectly aligns with no tilt from the normal angle of incidence. Otherwise, the MM elements m_{24} , m_{34} , m_{42} , and m_{43} may contain dispersions of the parasitic stress-induced linear birefringence, which, combined with any cuvette tilt, could interfere with the CD and ORD signals, leading to inaccuracies and potential misinterpretation.

To compare the MM elements in Eq. (5) with other experiments or simulations, we renormalize (4) to get CD $\Delta\epsilon$ and ORD $\Delta\theta$ in usual units,

$$\Delta\epsilon [\text{in L} \cdot \text{mol}^{-1} \cdot \text{cm}^{-1}] = \frac{4}{\ln 10} \frac{M}{dc} \chi [\text{in rad}], \quad (6a)$$

$$\Delta\theta [\text{in deg} \cdot \text{L} \cdot \text{mol}^{-1} \cdot \text{cm}^{-1}] = \frac{180}{\pi} \frac{M}{dc} \phi [\text{in rad}], \quad (6b)$$

where M is molar mass in $\text{g} \cdot \text{mol}^{-1}$, d is cuvette path length in cm, c is sample concentration in $\text{g} \cdot \text{L}^{-1}$, and the factor $180/\pi$ is a conversion from rad to degrees. The output of the CD spectroscopy measurements is usually given in degree; therefore, the normalization takes the form,

$$\Delta\epsilon [\text{in L} \cdot \text{mol}^{-1} \cdot \text{cm}^{-1}] = \frac{\pi}{180} \frac{4}{\ln 10} \frac{M}{dc} \chi [\text{in deg}]. \quad (7)$$

A detailed derivation of the factor $4/\ln 10$ is provided in Ref. [21]. Other

relations between quantities used in chiroptical spectroscopy and Mueller matrix (2) are provided in SI. The molar absorption coefficient ϵ is given in standard units $\text{L} \cdot \text{mol}^{-1} \cdot \text{cm}^{-1}$.

3. Results and discussion

3.1. MMP methodology demonstrated on Co-salen

This section details the methodology for chiroptical MMP measurements and data treatment, using Co-salen as an example. Fig. 3 illustrates the procedure. The chiroptical response reflects molecular P/M axial chirality affecting the d - d transitions, which are the most relevant for the spectra in visible (VIS) and NIR regions. For the transmission measurement of *S*- and *R*-Co-salen complexes in toluene solutions placed in a stress-free cuvette, we employed the MMP in a transmission setup at a normal angle of incidence. Because of the anticipated weak signals in the context of polarimetry, several modifications to the standard procedure were necessary.

The RC2 Woollam was calibrated in a standard way using a Si wafer with a well-defined SiO_2 thin film, which calibrates the ellipsometric system in both reflection and transmission modes. The calibration quality degrades over time – usually after several hours, but specific MM elements like m_{23} and m_{32} are affected much sooner and are more prone to temperature fluctuations. This instability is not optimal as it directly affects the ORD response given by Eq. (5). There are two possible solutions to this issue: re-calibrate the system after each measurement, but this approach does not ensure consistency in the calibration of critical MM elements due to potential random and systematic errors varying across calibrations. A more effective strategy involves measuring the MM response of the background – in our case, a cuvette filled with pure solvent – after each measurement and subtracting this from the sample data. Assuming the calibration is consistent between two consecutive measurements, this method ensures the correction of the measurement errors, allowing for stable and repeatable measurements of chiroptical spectra. We adjusted the acquisition times for each measurement to 300 s. Such a long acquisition is much more than regular ellipsometric measurements employing RC2 systems that can be done in less than a second; in 20 s for accurate analyses. While longer acquisition times enhance sensitivity, they also increase susceptibility to systematic errors. However, those are mitigated through background subtraction. At the same time, 300 s is short enough to avoid a change in systematic errors between the sample and background measurements. Measurements of many concentrations allow the exploitation of the entire operational range of the instrument, similar to classical ECD spectroscopy. Such an approach is somewhat unconventional in polarimetry and even more in reflection ellipsometry; however, it provides much more reliable results than the standard procedure.

Fig. 3 illustrates this methodology alongside a standard approach. We focus on the MMP chiroptical signal only within the NIR spectrum between 1000–1700 nm to simplify the explanation; the rest of the spectra are in Sec. S2. Fig. 3b and 3c display the CD and ORD averaged MM elements of Co-salens, each measured at a concentration of 5 mg/ml in a 10 mm cuvette. The signal averaging of m_{14} , m_{41} , and m_{23} , m_{32} enhances measurement sensitivity. The raw data already clearly reveal mirror symmetry in the CD and ORD spectra of the enantiomers. Fig. 3b indicates that the CD response is affected by significant systematic errors at 1000 nm due to a detector change and a lack of signal above 1660 nm. The ORD spectra in Fig. 3c exhibit local systematic errors around 1145 nm and 1385 nm and a significant unphysical drop in the spectra above 1620 nm. Such behavior of the m_{23} and m_{32} elements typically indicates weak signal. Indeed, part of the distorted spectra can be rectified by subtracting background signals from a cuvette with toluene, as depicted in Fig. 3d and 3e. The resulting corrected spectra (Fig. 3f and 3g) demonstrate that the systematic errors were nearly eliminated in both CD and ORD. In addition, the corrected ORD spectra include an

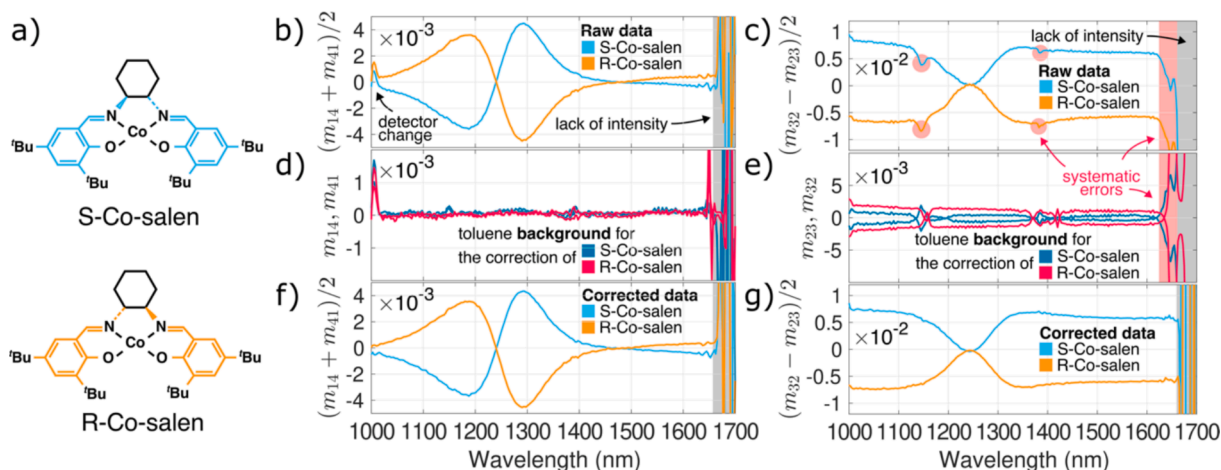


Fig. 3. Measurement methodology. a) S and R-Co-salen. b) CD and (c) ORD raw chiroptical signals of Co-salens. d) CD and (e) ORD of the toluene background. f) CD and (g) ORD chiroptical signals after the subtraction of the background.

additional 40 nm of chiroptical signal, extending the accessible spectral range up to 1660 nm. Furthermore, the background correction is necessitated even more since the background in m_{23} and m_{32} causes an offset in the sample's ORD and slightly alters its dispersion profile.

3.2. MMP and DFT analysis of Co-salen over UV-NIR spectrum

We compare the MMP measured spectra of Co-salen to traditional ECD experiments and ab-initio simulations. Fig. 4a and 4b compare the normalized CDs and ORDs of Co-salen acquired by MMP and ECD in two distinct solvents. The CDs and ORDs stitched from the NIR signal (>1000 nm in this case) discussed in Sec. 3.1, and the rest (<1000 nm

for MMP, <800 nm for ECD) for both MMP and ECD were obtained from concentrations detailed in Sec. 2; Fig. S1 displays additional details. The ORD cuts off at 600 nm due to high absorption below that point, affecting m_{23} and m_{32} but not so much the m_{14} and m_{41} elements, thus extending MMP coverage down to 480 nm. The resulting complex chiroptical signal accurately reflects mirror symmetry between enantiomers, is consistent with KK relations, and corresponds to the absorption profiles shown in Fig. 4c. The CD spectra in overlapping spectral regions for both experiments closely match; however, the MMP data are noisier below 600 nm. Section 4 addresses the specific reasons for this.

The chiroptical signal across the entire spectral range is consistent across different experiments and solvents, exhibiting only minor

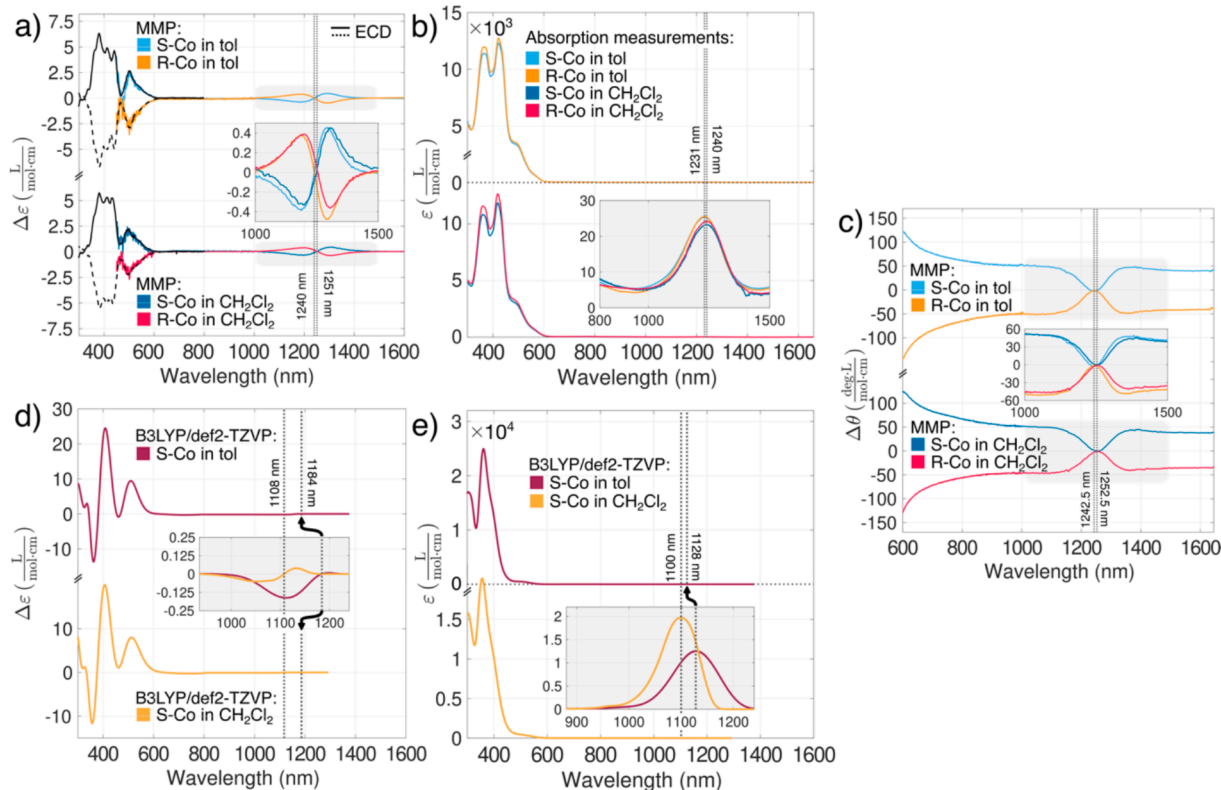


Fig. 4. CD (a), absorption (b), and ORD (c) experimental spectra of Co-salens dissolved in toluene (tol) and dichloromethane (CH_2Cl_2) with magnified NIR signals showing solvatochromism. Calculated CD (d) and absorption spectra (e) of S-Co-salen at B3LYP/def2-TZVP level with the vibrational resolution in toluene and dichloromethane. The inset shows magnified NIR chiroptical signal of both enantiomers.

wavelength and intensity variations in toluene and dichloromethane. While the UV–VIS spectrum dominates the amplitude variations, the NIR signal also shows a spectral shift by about 10 nm uniformly across CD, ORD, and absorption (Fig. 4a,b,c).

While the CD signal in the NIR region cannot be verified using a commercial ECD spectrometer, it is supported by vibronic spectral ab-initio simulations summarized in Fig. 4d,e. Electronic spectra calculated in the vertical approximation indicate one electronic transition in this region and replicate only the predominantly negative CD for the *S*-enantiomer, while inclusion of the vibrational splitting also provides the positive lobe. It should be noted, however, that the results vary across different functionals, basis sets and fine vibrational parameters.

Within 300–800 nm region, the (non-vibrationally resolved) calculated spectra overestimate the intensities if compared to the experiment but reproduce the experimental sign pattern reasonably well (Sec. S3 shows a detailed comparison). The theoretical absorption intensities and patterns are reasonably close to the experiment although there are discrepancies between the theoretical and experimental intensities suggesting that the complex possesses a complicated electronic structure and TD-DFT is unable to model it properly. The CAM-B3LYP and B3PW91 functionals performed similarly to B3LYP (cf. SI for detailed comparison).

For this part, we can summarize that MMP is the only available experimental method to us providing reliable access to the complex chiroptical response of Co-salen in the NIR region, uncovering spectral shifts with different solvents which can be, to some extent, confirmed by DFT simulations. Although the raw measured signals (Fig. 3) are close (and even beyond at parts of the spectra) to the sensitivity limit of 0.001 in the MM element of Woollam RC2-DI, we could push the instrument beyond its limits and demonstrate its advanced capabilities and versatility.

3.3. Co-EDDS, Kramers-Kronig analysis

In this section, we identify the key advantages of MMP's ability to access complex chiroptical signals using the toolbox of classical optics and we place the analyses in contrast to conventional measurements and simulations. For this purpose, we selected the *S*- and *R*-Co-EDDS chelate complex as another system (Fig. 5a) – a stable compound with strong chiroptical signals across UV, VIS, and resonance ROA spectra [81], making it a convenient standard for calibrating various spectroscopic instruments for chiroptical analyses [66].

Measurements at a single concentration of both enantiomers, as detailed in Section 2, were sufficient to acquire the MMP spectral response from 300–1700 nm (to support the methodology section, we

include the raw MM response in whole spectral range in SI, Sec. S4). The non-zero chiroptical signal is only up to 700 nm, which overlaps with the conventional ECD spectral range, and we thus limit our discussion to 300–700 nm part of the spectra.

The signal processing methodology for Co-EDDS closely follows that used in the Co-salen case, with one modification: instead of varying concentration, we used different path lengths of the cuvette (2, 5, and 10 mm) to avoid dilution of samples synthesized in very low volume. Fig. 6b displays the CD spectra obtained using MMP (averaged for all cuvettes) alongside a conventional spectrometer, showing spectra up to 700 nm. Signals for longer wavelengths were immeasurable/zero. Spectra below 300 nm are not obtained due to high absorption, Fig. 5d.

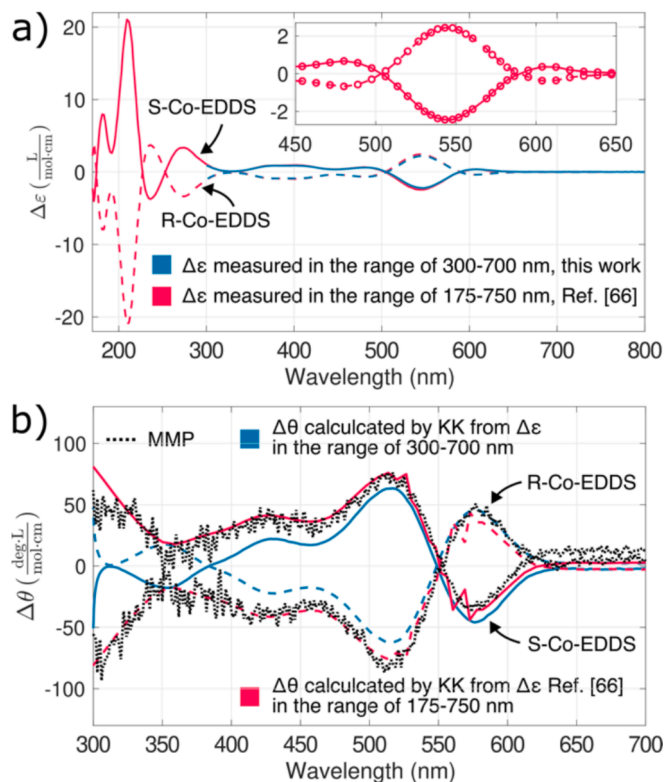


Fig. 6. Kramers-Kronig analysis of Co-EDDS chiroptical spectra. a) Different measurements of CD of Co-EDDS. CD data from Ref. [66] are also in the inset b) ORD calculated from the CD according to the Kramers-Kronig relations.

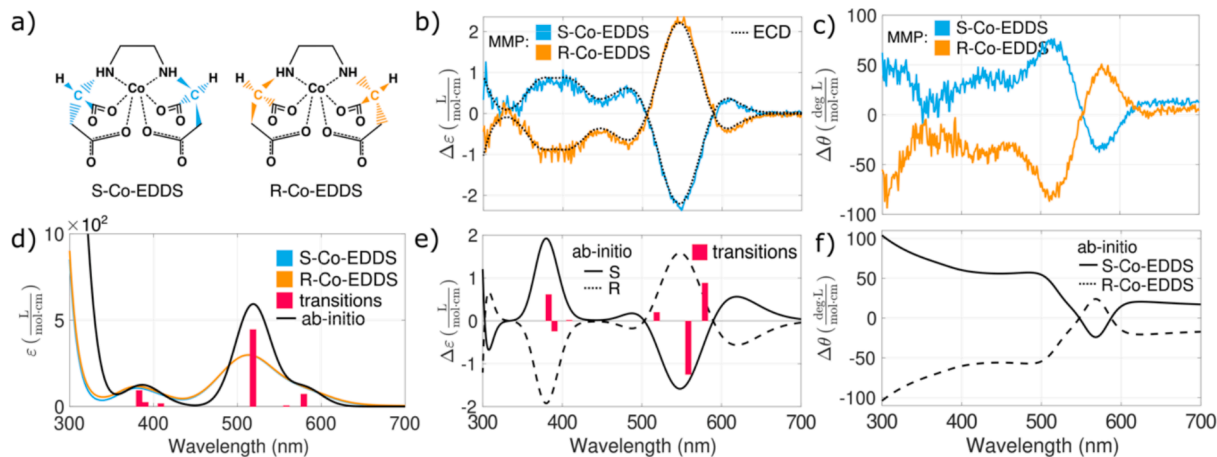


Fig. 5. a) *S* and *R*-Co-EDDS. b) MMP compared to traditional ECD measurements. c) ORD obtained with MMP. d) Experimental and theoretical calculated absorption of Co-EDDS chelates e) Simulated CD and individual electronic transitions for *S*-Co-EDDS. f) Simulated ORD.

The ellipsometric data are noisier than ECD, attributed to the instrument's lower sensitivity. Calculations reasonably reproduce the experimental absorption, CD, and ORD (Fig. 5b,c,e,f).

For deeper insight, we juxtapose MMP results with ab-initio calculations and Kramers-Kronig (KK) calculated spectra derived from measured CD spectra using equations [20,82]

$$\phi(\lambda) = \frac{2\lambda^2}{\pi} \wp \int_0^\infty \frac{\chi(\lambda')}{\lambda'(\lambda'^2 - \lambda^2)} d\lambda', \quad (8a)$$

$$\chi(\lambda) = -\frac{2\lambda}{\pi} \wp \int_0^\infty \frac{\phi(\lambda')}{(\lambda'^2 - \lambda^2)} d\lambda'. \quad (8b)$$

The symbol \wp denotes the Cauchy principal value of the integrals, λ is the wavelength at which the optical properties are being calculated, and λ' is the variable of integration representing the wavelength of the right-hand side spectra. Since the ORD (8a) is caused by the absorption (8b) via the causality theorem, we solely derive ORD spectra from CD spectra using Eq. (8a) [82] and with help of Eqs. (6) and (7). The form of the KK relations (8) follows the well-known set given, for example, in Ref. [21].

Fig. 6b compares two different calculated ORD spectra from two sets of CDs shown in Fig. 6a. The blue curves correspond to the ECD measurements depicted in Fig. 5b, the red curves are based on the data from Ref. [66]. The comparison of both sets of complex chiroptical signals demonstrates that generating ORD curves solely from ECD data within the 300–700 nm range (blue curve) leads to unphysical behavior at the ends of the used wavelength span. This issue stems from the inherent feature of KK relations, which require integration over a semi-infinite spectrum from 0 to ∞ . For accurate KK transformation of CD into ORD spectra, measurements must extend beyond the accessible spectral range. This extra information is especially critical in the UV region, where numerous electronic transitions may lead to complicated CD, thereby preventing reasonable extrapolation estimates beyond the measured short-wavelength end of the spectrum. Additionally, the samples are often highly absorptive in the UV region, further complicating the access to CD information. The estimate is easier to make for longer wavelengths where the CD signal diminishes to zero, allowing for an extrapolation. However, even this method is not universally applicable: for Co-salen, some CD signal persists into the NIR. In this view, the ability of MMP to directly measure both KK counterparts of the chiroptical spectrum is impeccable. Furthermore, by utilizing experimental data from Ref. [66], which spans a 175–750 nm range at a 0.056 mM R-Co-EDDS concentration, we achieved a better KK transformation (red curve in Fig. 6b). It closely replicates and thus validates the MMP experimental results. The sawtooth-like oscillations in the ORD red

curves around 525 nm and 560 nm are caused by numerical instabilities due to low and uneven spectral resolution of the literature-retrieved CD data (inset of Fig. 6a). The ORD spectra from the KK transformation, MMP measurements, and ECD experiments still outperform those obtained by DFT.

3.4. Limits of MMP for AlCl-salen and MnCl-salen

Figs. 7 and 8 Display the chiroptical spectra of AlCl-salen and MnCl-salen, respectively. For AlCl-salen, the measured (Fig. 7b) and simulated CD spectra (Fig. 7e) are in reasonable agreement. Four electronic transitions are predicted within the visible region, not resolved in absorption (Fig. 8d). Below 300 nm, where significant absorption prevents reliable measurements, a more complex chiroptical response is expected due to numerous transitions. This is indicated in Fig. 7d,e.

In contrast, MnCl-salen gives a signal in VIS-NIR regions (Fig. 8) due to multiple *d-d* transitions (parts d,e). Due to high UV absorption, the spectra are measured from 300 nm. Above 1100 nm, the material is transparent.

Although detailed chiroptical responses of AlCl-salen and MnCl-salens vary, there are common aspects. In both cases, the simulated CD ab-initio spectra reasonably match the experiment. For both compounds, the alignment between MMP and ECD is excellent from 450 nm upwards, but unlike AlCl-salen, ellipsometric data mostly follow only the CD trends at the blue end of the VIS spectrum. Both compounds also give noisy, distorted ORD spectra (Figs. 7c, 8c) but still reflect some KK consistency. The reasons are discussed in the next Section.

4. Discussion on the RC2-MMP sensitivity

The primary challenge in RC2-MMP arises from limited sensitivity, especially within the UV spectral region. For AlCl and MnCl salen complexes, the critical part of the chiroptical response is observed below 450 nm, coinciding with the region of strongest absorption. In this spectral range, the sensitivity of the measurement setup is significantly lower, reducing the reliability of extracted CD and, more notably, ORD. The lower sensitivity predominantly impacts the MM elements m_{23} and m_{32} , which are also highly susceptible to temperature fluctuations.

In contrast, measurements of Co-salen complexes extending from the UV to the near-infrared (NIR) region demonstrate that RC2-MMP can accurately capture genuine chiroptical signals up to 1700 nm. The sensitivity achieved through careful background subtraction and extended acquisition times (as illustrated in Fig. 3) can exceed the system's guaranteed MM element accuracy of 10^{-3} . Moreover, Co-EDDS complexes exhibit dissymmetry factor values comparable to those of AlCl and MnCl salen complexes, but notably with approximately an

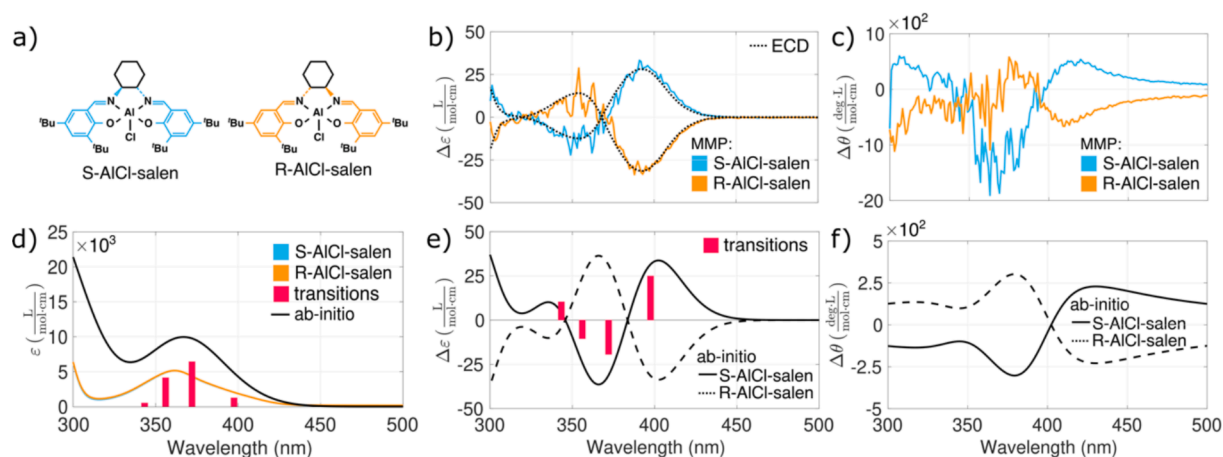


Fig. 7. a) S and R-AlCl-salen. b) MMP compared to traditional ECD measurements. c) ORD obtained with MMP. d) Experimental and theoretical calculated absorption e) Simulated CD and individual electronic transitions. f) Simulated ORD.

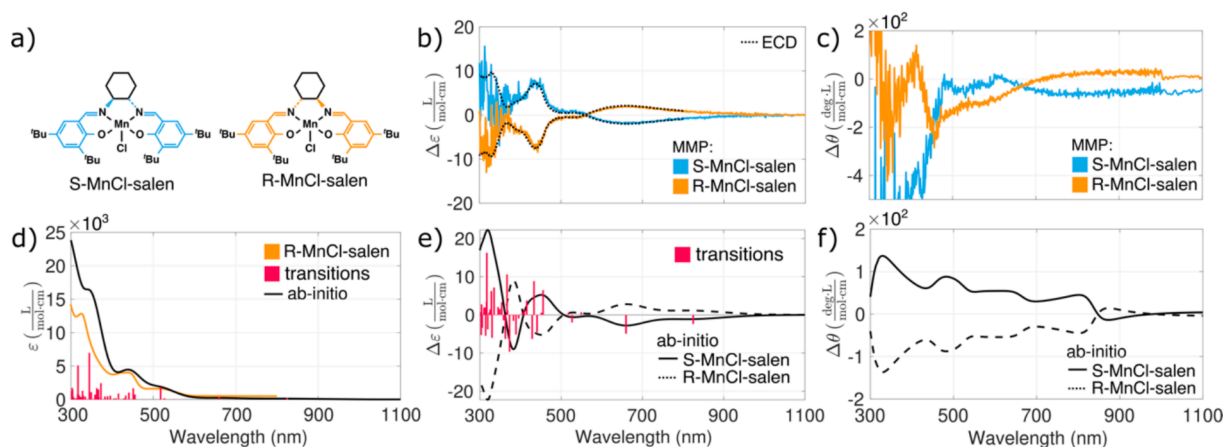


Fig. 8.) S and R-MnCl-salen. b) MMP compared to traditional ECD measurements. c) ORD obtained with MMP. d) Experimental and theoretical calculated absorption. e) Simulated CD and individual electronic transitions. f) Simulated ORD.

order of magnitude lower absorption intensities.

The ellipsometer with dual-rotating compensators that was used is less sensitive than those using photo-elastic modulators or liquid crystals. This reduced sensitivity is due to the fixed retardance of the compensators, which are precisely adjusted to cover the entire Poincaré sphere – a representation of all polarized light states. As a result, the sensitivity to each polarization state is uniform, meaning there is no way to enhance sensitivity in specific regions of the Poincaré sphere, particularly at the poles corresponding to left and right circular polarizations.

On the other hand, phase-modulating ellipsometers with fixed components provide better signal-to-noise ratios by eliminating potential mechanical instabilities and can improve sensitivity to selected polarizations. These systems sequentially scan one wavelength at a time, enabling better detection of phase differences between circular polarizations. Employing four PEMs in MMP further improves the sensitivity and mainly aims for reliable extraction of weak signals [83,84]. Traditional commercial spectrometers like ECD typically use PEM or pair of PEMs, contributing to their higher accuracy in measuring CD signals compared to the Woollam RC2-DI. ECD is more practical for routine UV–VIS chiroptical measurements of solutions, while HAUP may serve as a potential alternative for more specialized, non-routine analyses.

In summary, RC2 MMP could be used for classical tasks in analytical chemistry. A significant advantage is the compatibility with CCD detection, allowing simultaneous measurements across the entire UV–NIR spectrum in a fraction of a second. The proposed methodology applies to all Mueller matrix-based polarimeters but currently requires longer acquisition times. Technological advancements – including the development of super-continuum light sources, polarizers with ultra-high extinction ratios, highly precise motorization, and compensators free of material-induced parasitic polarization – alongside improved temperature stabilization, can significantly enhance signal-to-noise ratios and thus reduce measurement times. Nonetheless, such technological enhancements would similarly benefit other polarization-based measurement techniques. Consequently, due to intrinsic instrument design considerations, the inherent sensitivity of RC2-based systems to chiroptical signals will always remain lower compared to specialized instrumentation. In spite of these problems, custom RC2 MMP and MMSE systems have the potential to become valuable tools for routine and exceptionally rapid chiroptical measurements, capable of reliably monitoring equilibrium, time-varying, in-situ, and in-vivo complex chiroptical signals.

5. Conclusions

In this work, we have applied the commercially available Mueller

matrix spectroscopic ellipsometer Woollam RC2-DI in transmission configuration referred to as Mueller matrix polarimetry for the chiroptical analysis of metal salen-chelate organic complexes. We established an optimal and universally applicable measurement methodology (illustrated in Fig. 3), that can be easily adjusted for specific requirements of samples in form of isotropic solution and various experimental instrumentations. We analyzed the complex chiroptical responses (CD and ORD), which we compared to a more established ECD technique in this field to validate the results obtained with MMP. In addition, the ab-initio calculations were applied to (i) further validate the findings collected via the MMP and (ii) unravel the mechanisms causing the chiroptical response of each studied compound. At this point, we highlight that our intention was not to challenge the traditional chiroptical methods, aim for competition, and claim superiority of MMP; instead, we attempted to portray the MMP with all the benefits it brings into the established field, outline its potential future perspectives, and, with the same importance, point out drawbacks this method may carry. Along the methodology and demonstration of MMP in classical tasks of analytic chemistry, the original results of this work are as follows:

- We have acquired the chiroptical response of each salen-chelate complex over a spectral range spanning from 300 nm to 1660 nm, which is broader than the spectrum accessible by most commercial ECD spectrometers. The lower limit is due to absorption of sample and sensitivity of used setup; the MMP used in this work enables 193 nm. The accessibility to the NIR region allowed for the experimental characterization and subsequent DFT modeling of the chiroptical signal of Co-salens in their neutral form.
- Of course, some commercially available ECD spectrometers cover an extended spectral range, such as the ellipsometer used in this work; however, these instruments are considerably expensive, single-purpose, and less versatile.
- The MMP measures a complex chiroptical response within a single set of measurements (sample and background). The resulting CD and ORD spectra obey KK relations, which makes them self-consistent. This fact potentially enables a robust characterization of chiroptical spectra even for compounds for which only one enantiomer is accessible. The KK consistency guarantees recognition of a physically significant signal from parasitic effects or systematic errors from, for instance, linear birefringence induced by the instrument or sample itself (sub-optimal cuvette).

Simultaneous measurement of CD and ORD signals can open up possibilities for study of non-equilibrium processes, such as chiral reaction kinetics, mutarotations, chiral crystallization, or Belousov-Zhabotinskii-type reactions with chiral molecules. However, high

absorptions might hinder the observation of CD time responses. Observing the ORD spectrum in a different spectral region corresponding to the same phenomenon can address this issue.

One may be tempted to convert the CD signal obtained with ECD into ORD through KK relations, sidestep thus the MMP and assuming this approach to be sufficiently accurate. This is a pitfall. We demonstrated in Fig. 6, this may lead to unphysical spectral profiles or, to maintain the physical significance, will substantially reduce the viable spectral range of the sought response function.

- We unveiled a potential drawback of the current Woollam RC2-DI system: overall lower sensitivity of the method, particularly over UV and a portion of the VIS spectrum (up to 450 nm) due to the low intensity of source lamps over this spectral range. Other methods like ECD and HAUP are still more suitable for equilibrium chiroptical measurements within this part of spectrum.

CRedit authorship contribution statement

Daniel Vala: Conceptualization, Data curation, Formal analysis, Investigation, Methodology, Visualization, Writing – original draft, Writing – review & editing. **Jiří Zdráhala:** Data curation, Formal analysis, Investigation, Methodology, Writing – original draft. **Jana Hudecová:** Data curation, Formal analysis, Investigation, Methodology, Writing – review & editing. **Hana Šestáková:** Investigation, Resources. **Jaroslav Šebestík:** Investigation, Resources. **David Kopečný:** Resources. **Josef Kapitán:** Methodology, Resources, Validation, Writing – review & editing. **Petr Bour:** Conceptualization, Methodology, Supervision, Validation, Writing – original draft, Writing – review & editing. **Kamil Postava:** Methodology, Funding acquisition, Project administration, Supervision, Validation, Writing – review & editing.

Funding

The authors acknowledge the partial support of the following projects: project No. 22-33060S of the Czech Science Foundation (GAČR); project No. CZ.02.01.01/00/22_008/0004631- “Materials and Technologies for Sustainable Development”, funded by the European Union and the state budget of the Czech Republic within the framework of the Jan Amos Komenský Operational Program; project REFRESH – Research Excellence For Region Sustainability and High-tech Industries project number CZ.10.03.01/00/22_003/0000048 via the Operational Programme Just Transition; Student Grant System SP2024/086. This work was supported by the Ministry of Education, Youth and Sports of the Czech Republic through the e-INFRA CZ (ID:90254).

Declaration of competing interest

The authors declare that they have no known competing financial interests or personal relationships that could have appeared to influence the work reported in this paper.

Acknowledgements

It is a great pleasure for Daniel Vala to express gratitude to Daniel Cvejn for his helpful discussions on chiral chemistry.

Appendix A. Supplementary data

Supplementary data to this article can be found online at <https://doi.org/10.1016/j.saa.2025.126279>.

Data availability

The data that support the findings of this study are openly available in zenodo at <https://zenodo.org/records/14601157>, reference number 14601157.

References

- [1] M. Singh, S. Sethi, R. Bhushan, Liquid chromatographic methods for separation, determination, and bioassay of enantiomers of etodolac: A review, *J. Sep. Sci.* 43 (2020) 18–30.
- [2] L.A. Nguyen, H. He, C. Pham-Huy, Chiral drugs: an overview, *Int. J. Biomed. Sci.* 2 (2006) 85–100.
- [3] M.E. Franks, G.R. Macpherson, W.D. Figg, Thalidomide, *Lancet* 363 (2004) 1802–1811.
- [4] N. Vargesson, Thalidomide-induced teratogenesis: History and mechanisms, *Birth Defects Res. C Embryo Today* 105 (2015) 140–156.
- [5] H.D. Flack, G. Bernardinelli, The use of X-ray crystallography to determine absolute configuration, *Chirality: The Pharmacological, Biological, and Chemical Consequences of Molecular Asymmetry* 20 (2008) 681–690.
- [6] Á. Valentín-Pérez, P. Rosa, E.A. Hillard, M. Giorgi, Chirality determination in crystals, *Chirality* 34 (2022) 163–181.
- [7] D.W. Armstrong, Optical isomer separation by liquid chromatography, *Anal. Chem.* 59 (1987) 84A–91A.
- [8] V. Schurig, Separation of enantiomers by gas chromatography, *J. Chromatogr. A* 906 (2001) 275–299.
- [9] X. Yu, Z.-P. Yao, Chiral recognition and determination of enantiomeric excess by mass spectrometry: A review, *Anal. Chim. Acta* 968 (2017) 1–20.
- [10] T.J. Ward, K.D. Ward, Chiral separations: a review of current topics and trends, *Anal. Chem.* 84 (2012) 626–635.
- [11] P. Lazzaretti, Chiral discrimination in nuclear magnetic resonance spectroscopy, *J. Phys. Condens. Matter* 29 (2017) 443001.
- [12] P. Lesot, C. Aroulanda, H. Zimmermann, Z. Luz, Enantiotopic discrimination in the NMR spectrum of prochiral solutes in chiral liquid crystals, *Chem. Soc. Rev.* 44 (2015) 2330–2375.
- [13] P.L. Polavarapu, Renaissance in chiroptical spectroscopic methods for molecular structure determination, *Chem. Rec.* 7 (2007) 125–136.
- [14] M. Krupová, J. Kessler, P. Bour, Recent trends in chiroptical spectroscopy: theory and applications of vibrational circular dichroism and Raman optical activity, *Chem plus Chem* 85 (2020) 561–575.
- [15] M. Halat, K. Pajor, R. Baranski, M. Baranska, (Resonance) Raman optical activity among chiroptical spectroscopies: Quo vadis? *J. Raman Spectrosc.* 55 (2024) 539–548.
- [16] P. Michal, J. Kapitán, J. Kessler, P. Bour, Low-frequency Raman optical activity provides insight into the structure of chiral liquids, *PCCP* 24 (2022) 19722–19733.
- [17] R.A. Lombardi, L.A. Nafie, Observation and calculation of vibrational circular birefringence: A new form of vibrational optical activity, *Chirality: The Pharmacological, Biological, and Chemical Consequences of Molecular Asymmetry* 21 (2009) E277–E286.
- [18] W. Moffitt, A. Moscovitz, Optical activity in absorbing media, *J. Chem. Phys.* 30 (1959) 648–660.
- [19] P.L. Polavarapu, Kramers-Kronig transformation for optical rotatory dispersion studies, *Chem. Eur. J.* 109 (2005) 7013–7023.
- [20] M.W. Brockman, A. Moscovitz, Macroscopic sum rules in natural optical activity, *Mol. Phys.* 43 (1981) 1385–1393.
- [21] L.A. Nafie, *Vibrational Optical Activity: Principles and Applications*, John Wiley & Sons, 2011.
- [22] D. Franta, Symmetry of linear dielectric response tensors: dispersion models fulfilling three fundamental conditions, *J. Appl. Phys.* 127 (2020) 223101–223117.
- [23] X. Xie, J.D. Simon, Picosecond time-resolved circular dichroism spectroscopy: experimental details and applications, *Rev. Sci. Instrum.* 60 (1989) 2614–2627.
- [24] C.F. Zhang, J.W. Lewis, R. Cerpa, I.D. Kuntz, D.S. Kliger, Nanosecond circular dichroism spectral measurements: extension to the far-ultraviolet region, *J. Phys. Chem.* 97 (1993) 5499–5505.
- [25] I. Eom, S.-H. Ahn, H. Rhee, M. Cho, Single-shot electronic optical activity interferometry: power and phase fluctuation-free measurement, *Phys. Rev. Lett.* 108 (2012) 103901.
- [26] F. Auvray, D. Denetiere, A. Giuliani, F. Jamme, F. Wien, B. Nay, S. Zirah, F. Polack, C. Meneglier, B. Lagarde, Time resolved transient circular dichroism spectroscopy using synchrotron natural polarization, *Struct. Dyn.* 6 (2019) 1–6.
- [27] D. Vala, M. Mićica, K. Postava, J. Pištora, Optical activity temperature-dependent measurements of chiral solutions using Mueller matrix spectroscopic ellipsometry, in: 21st Czech-Polish-Slovak Optical Conference on Wave and Quantum Aspects of Contemporary Optics, 2018, pp. 54–60.
- [28] D. Vala, M. Mićica, D. Cvejn, K. Postava, Broadband Mueller ellipsometer as an all-in-one tool for spectral and temporal analysis of mutarotation kinetics, *RSC Adv.* 13 (2023) 6582–6592.
- [29] K. Hiramatsu, T. Nagata, Communication: Broadband and ultrasensitive femtosecond time-resolved circular dichroism spectroscopy, *J. Chem. Phys.* 143 (2015) 121102.
- [30] J. Kobayashi, Y. Uesu, A new optical method and apparatus HAUP for measuring simultaneously optical activity and birefringence of crystals. I. Principles and construction, *J. Appl. Cryst.* 16 (1983) 204–211.
- [31] J. Kobayashi, T. Asahi, Development of HAUP and its applications to various kinds of solids, in: A. Lakhtakia, W.S. Weiglhofer, R.F. Messier (Eds.), *Proceedings Volume 4097, Complex Mediums*, SPIE, 2000, pp. 25–39.
- [32] A. Takanabe, M. Tanaka, K. Johmoto, H. Uekusa, T. Mori, H. Koshima, T. Asahi, Optical activity and optical anisotropy in photomechanical crystals of chiral salicylidene-phenylethylamines, *J. Am. Chem. Soc.* 138 (2016) 15066–15077.
- [33] K. Nakagawa, A.T. Martin, S.M. Nichols, V.L. Murphy, B. Kahr, T. Asahi, Optical activity anisotropy of benzil, *J. Phys. Chem. C* 121 (2017) 25494–25502.

- [34] J. Kobayashi, H. Kumomi, K. Saito, Improvement of the accuracy of HAUP, high-accuracy universal polarimeter: application to ferroelectric [N(CH₃)₄]ZnCl₄, *J. Appl. Cryst.* 19 (1986) 377–381.
- [35] K. Nakagawa, T. Asahi, Determination of the Faraday rotation perpendicular to the optical axis in uniaxial CeF₃ crystal by using the Generalized-High Accuracy Universal Polarimeter, *Sci. Rep.* 9 (2019) 18453.
- [36] T. Asahi, M. Tanaka, K. Nakagawa, Y. Terasawa, K. Ishikawa, A. Takanabe, H. Koshima, B. Kahr, Chiroptical studies on anisotropic condensed matter: principle and recent applications of the generalized-high accuracy universal polarimeter, in: *Crystal Growth and Chirality-Technologies and Applications*, IntechOpen, 2022.
- [37] A. Takanabe, H. Koshima, T. Asahi, Fast-type high-accuracy universal polarimeter using charge-coupled device spectrometer, *AIP Adv.* 7 (2017) 025209–025214.
- [38] X. Chen, H. Gu, L. Jiamin, C. Chen, S. Liu, Advanced Mueller matrix ellipsometry: Instrumentation and emerging applications, *Sci. China Technol. Sci.* 65 (2022) 1–24.
- [39] D.E. Aspnes, Spectroscopic ellipsometry — Past, present, and future, *Thin Solid Films* 571 (2014) 334–344, <https://doi.org/10.1016/j.tsf.2014.03.056>.
- [40] E. García-Caurel, R. Ossikovski, M. Foldyna, A. Pierangelo, B. Drévilion, A. De Martino, Advanced Mueller ellipsometry instrumentation and data analysis, in: *Ellipsometry at the Nanoscale*, Springer, Berlin Heidelberg, 2013, pp. 31–143, <https://books.google.cz/books?id=SesAAAAQBAJ>.
- [41] A. Cumurcu, X. Feng, L. Dos Ramos, M.A. Hempenius, P. Schön, G.J. Vancso, Sub-nanometer expansions of redox responsive polymer films monitored by imaging ellipsometry, *Nanoscale* 6 (2014) 12089–12095, <https://doi.org/10.1039/C4NR02852J>.
- [42] Y. Karmakov, A. Paskaleva, D. Spassov, Depth profiling of very thin HfO₂/Al₂O₃ stacks by ellipsometry, *J. Phys. Conf. Ser.* 2240 (2022) 12049, <https://doi.org/10.1088/1742-6596/2240/1/012049>.
- [43] M. Hemmat, S. Ayari, M. Mićić, H. Vergnet, S. Guo, M. Arfaoui, X. Yu, D. Vala, A. Wright, K. Postava, others, Layer-controlled nonlinear terahertz valleytronics in two-dimensional semimetal and semiconductor PtSe₂, *InfoMat* 5 (2023) e12468.
- [44] C. He, H. He, J. Chang, B. Chen, H. Ma, M.J. Booth, Polarisation optics for biomedical and clinical applications: a review, *Light Sci. Appl.* 10 (2021) 1–20, <https://doi.org/10.1038/s41377-021-00639-x>.
- [45] O. Rodríguez-Núñez, P. Schucht, E. Hewer, T. Novikova, A. Pierangelo, Polarimetric visualization of healthy brain fiber tracts under adverse conditions: ex vivo studies, *Biomed. Opt. Express* 12 (2021) 6674–6685, <https://doi.org/10.1364/BOE.439754>.
- [46] M. Kupinski, M. Boffety, F. Goudail, R. Ossikovski, A. Pierangelo, J. Rehbinder, J. Vizet, T. Novikova, Polarimetric measurement utility for pre-cancer detection from uterine cervix specimens, *Biomed. Opt. Express* 9 (2018) 5691–5702, <https://doi.org/10.1364/BOE.9.005691>.
- [47] O. Herrfurth, S. Richter, M. Rebarz, S. Espinoza, J. Zúñiga-Pérez, C. Deparis, J. Leveillee, A. Schleife, M. Grundmann, J. Andreasson, R. Schmidt-Grund, Transient birefringence and dichroism in ZnO studied with fs-time-resolved spectroscopic ellipsometry, *Phys. Rev. Res.* 3 (2021) 13246, <https://doi.org/10.1103/PhysRevResearch.3.013246>.
- [48] S. Richter, O. Herrfurth, S. Espinoza, M. Rebarz, M. Kloz, J.A. Leveillee, A. Schleife, S. Zollner, M. Grundmann, J. Andreasson, R. Schmidt-Grund, Ultrafast dynamics of hot charge carriers in an oxide semiconductor probed by femtosecond spectroscopic ellipsometry, *New J. Phys.* 22 (2020) 83066, <https://doi.org/10.1088/1367-2630/aba7f3>.
- [49] X. Chen, Q. Sun, J. Wang, H. Lindley-Hatcher, E. Pickwell-MacPherson, Exploiting complementary terahertz ellipsometry configurations to probe the hydration and cellular structure of skin in vivo, *Adv. Photonics Res.* 2 (2021) 2000024, <https://doi.org/10.1002/adpr.202000024>.
- [50] J. Vizet, J. Rehbinder, S. Deby, S. Roussel, A. Nazac, R. Soufan, C. Genestie, C. Haie-Meder, H. Fernandez, F. Moreau, A. Pierangelo, In vivo imaging of uterine cervix with a Mueller polarimetric colposcope, *Sci. Rep.* 7 (2017) 1–12, <https://doi.org/10.1038/s41598-017-02645-9>.
- [51] L. Halagačka, Z. Gelnarová, M. Al-Ghazaiat, I. Florea, J. Horníček, K. Postava, M. Foldyna, Tin reduction from fluorine doped tin oxide for silicon nanowire-based solar energy harvesting and storage, *Opt. Express* 29 (2021) 31465–31477, <https://doi.org/10.1364/OE.435500>.
- [52] Z. Mrázková, I.P. Sobkowicz, M. Foldyna, K. Postava, I. Florea, J. Pištora, P.R. i Cabarrocas, Optical properties and performance of pyramidal texture silicon heterojunction solar cells: key role of vertex angles, *Prog. Photovolt. Res. Appl.* 26 (2018) 369–376, <https://doi.org/10.1002/pip.2994>.
- [53] R. Sachse, M. Moor, R. Kraehnert, V.-D. Hodoroaba, A. Hertwig, Ellipsometry-based approach for the characterization of mesoporous thin films for H₂ technologies, *Adv. Eng. Mater.* (2022) 2101320, <https://doi.org/10.1002/adem.202101320>.
- [54] V.M. Bjelland, N. Hale, N. Schwarz, D. Vala, J. Høvik, M. Kildemo, Diffractive order Mueller matrix ellipsometry for the design and manufacture of polarization beam splitting metasurfaces, *Opt. Express* 32 (2024) 703–721.
- [55] O. Arteaga, J. Freudenthal, B. Kahr, Reckoning electromagnetic principles with polarimetric measurements of anisotropic optically active crystals, *Appl. Crystallogr.* 45 (2012) 279–291.
- [56] N.J. Podraza, S.M. Pursel, C. Chen, M.W. Horn, R.W. Collins Jr, Analysis of the optical properties and structure of serial bi-deposited TiO₂ chiral sculptured thin films using Mueller matrix ellipsometry, *J. Nanophotonics* 2 (2008) 21930.
- [57] M. Schulz, J. Zablocki, O.S. Abdullaeva, S. Brück, F. Balzer, A. Lützen, O. Arteaga, M. Schiek, Giant intrinsic circular dichroism of prolinol-derived squaraine thin films, *Nat. Commun.* 9 (2018) 2413.
- [58] H. Hu, S. Sekar, W. Wu, Y. Battie, V. Lemaire, O. Arteaga, L.V. Poulidakos, D. J. Norris, H. Giessen, G. Decher, others, Nanoscale bouligand multilayers: giant circular dichroism of helical assemblies of plasmonic 1D nano-objects, *ACS Nano* 15 (2021) 13653–13661.
- [59] H. Arwin, R. Magnusson, J. Landin, K. Järrendahl, Chirality-induced polarization effects in the cuticle of scarab beetles: 100 years after Michelson, *Phil. Mag.* 92 (2012) 1583–1599.
- [60] O. Arteaga, Natural optical activity vs circular Bragg reflection studied by Mueller matrix ellipsometry, *Thin Solid Films* 617 (2016) 14–19.
- [61] O. Arteaga, A. Arango-Restrepo, D. Barragán, R. Ossikovski, J.M. Rubí, In situ study of chiral symmetry breaking in sodium chlorate solutions by Mueller matrix polarimetry, *Chirality* 35 (2023) 700–707.
- [62] O. Arteaga, A. Canillas, R. Purrello, J.M. Ribó, Evidence of induced chirality in stirred solutions of supramolecular nanofibers, *Opt. Lett.* 34 (2009) 2177–2179.
- [63] O. Arteaga, Z. El-Hachemi, A. Canillas, J.M. Ribó, Transmission Mueller matrix ellipsometry of chirality switching phenomena, *Thin Solid Films* 519 (2011) 2617–2623.
- [64] E.N. Jacobsen, W. Zhang, A.R. Muci, J.R. Ecker, L. Deng, Highly enantioselective epoxidation catalysts derived from 1, 2-diaminocyclohexane, *J. Am. Chem. Soc.* 113 (1991) 7063–7064.
- [65] S. Singh, B. Phukan, C. Mukherjee, A. Verma, Salen ligand complexes as electrocatalysts for direct electrochemical reduction of gaseous carbon dioxide to value added products, *RSC Adv.* 5 (2015) 3581–3589.
- [66] A. Damianoglou, E.J. Crust, M.R. Hicks, S.E. Howson, A.E. Knight, J. Ravi, P. Scott, A. Rodger, A new reference material for UV-visible circular dichroism spectroscopy, *Chirality* 20 (2008) 1029–1038, <https://doi.org/10.1002/chir.20566>.
- [67] A. Kochem, H. Kalso, B. Baptiste, H. Arora, C. Philouze, O. Jarjayes, H. Vezin, D. Luneau, M. Orio, F. Thomas, Ligand contributions to the electronic structures of the oxidized cobalt (II) salen complexes, *Inorg. Chem.* 51 (2012) 10557–10571.
- [68] T. Kurahashi, H. Fujii, Unique ligand-radical character of an activated cobalt salen catalyst that is generated by aerobic oxidation of a cobalt (II) salen complex, *Inorg. Chem.* 52 (2013) 3908–3919.
- [69] R.M. Clarke, K. Herasymchuk, T. Storr, Electronic structure elucidation in oxidized metal-salen complexes, *Coord. Chem. Rev.* 352 (2017) 67–82.
- [70] J.A. Neal, N.J. Rose, Stereospecific ligands and their complexes. I. A cobalt (III) complex of ethylenediaminedisuccinic acid, *Inorg. Chem.* 7 (1968) 2405–2412.
- [71] M.J. Frisch, G.W. Trucks, H.B. Schlegel, G.E. Scuseria, M.A. Robb, J.R. Cheeseman, G. Scalmani, V. Barone, G.A. Petersson, H. Nakatsuji, et al., Gaussian16 Revision C.01 (2016).
- [72] A.D. Becke, Density-functional thermochemistry. I. The effect of the exchange-only gradient correction, *J. Chem. Phys.* 96 (1992) 2155–2160.
- [73] R. Krishnan, J.S. Binkley, R. Seeger, J.A. Pople, Self-consistent molecular orbital methods. XX. A basis set for correlated wave functions, *J. Chem. Phys.* 72 (1980) 650–654.
- [74] T. Clark, J. Chandrasekhar, G.W. Spitznagel, P.V.R. Schleyer, Efficient diffuse function-augmented basis sets for anion calculations. III. The 3-21+ G basis set for first-row elements, Li–F, *J. Comput. Chem.* 4 (1983) 294–301.
- [75] F. Weigend, R. Ahlrichs, Balanced basis sets of split valence, triple zeta valence and quadruple zeta valence quality for H to Rn: Design and assessment of accuracy, *PCCP* 7 (2005) 3297–3305.
- [76] T. Yanai, D.P. Tew, N.C. Handy, A new hybrid exchange–correlation functional using the Coulomb-attenuating method (CAM-B3LYP), *Chem. Phys. Lett.* 393 (2004) 51–57.
- [77] F.J.A. Ferrer, F. Santoro, Comparison of vertical and adiabatic harmonic approaches for the calculation of the vibrational structure of electronic spectra, *PCCP* 14 (2012) 13549–13563.
- [78] O. Arteaga, Mueller matrix polarimetry of anisotropic chiral media, PhD Thesis, Barcelona, 2010. <https://www.mmpolarimetry.com/phd-thesis/> (accessed February 27, 2025).
- [79] R.C. Jones, A new calculus for the treatment of optical systems. VII. Properties of the N-matrices, *J. Opt. Soc. Am.* 38 (1948) 671–685.
- [80] J. Schellman, H.P. Jensen, Optical spectroscopy of oriented molecules, *Chem. Rev.* 87 (1987) 1359–1399.
- [81] Q. Yang, J. Bloino, H. Šestáková, J. Šebestík, J. Kessler, J. Hudecová, J. Kapitán, P. Bouř, Combination of resonance and non-resonance chiral Raman scattering in a cobalt (III) complex, *Angew. Chem.* 135 (2023) e202312521.
- [82] K. Ohta, H. Ishida, Comparison among several numerical integration methods for Kramers-Kronig transformation, *Appl. Spectrosc.* 42 (1988) 952–957.
- [83] O. Arteaga, J. Freudenthal, B. Wang, B. Kahr, Mueller matrix polarimetry with four photoelastic modulators: theory and calibration, *Appl. Opt.* 51 (2012) 6805–6817.
- [84] S. Alali, A. Gribble, I. Alex Vitkin, Rapid wide-field Mueller matrix polarimetry imaging based on four photoelastic modulators with no moving parts, *Opt. Lett.* 41 (2016) 1038–1041.